Colloid Polym Sci (2014) 292:2475–2484
DOI 10.1007/s00396-014-3260-6

ORIGINAL CONTRIBUTION

Compressed antisolvent process for polymer coating of drug-loaded aerogel nanoparticles and study of the release behavior

Nerea Murillo-Cremaes · Pascale Subra-Paternault · Javier Saurina · Anna Roig · Concepción Domingo

Received: 3 December 2013 / Revised: 25 April 2014 / Accepted: 9 May 2014 / Published online: 6 June 2014

Abstract The overall objective of the present work was to modulate the release behavior of drug-impregnated silica particles from almost instantaneous release to a more sustained delivery, prolonged during several hours. Triflusal was chosen as a model drug of the low biodisponibility type. The process is based in the coating with Eudragit® RL 100 polymer of aerogel-like silica particles. Materials were processed in compressed CO_2 by using the batch and semicontinuous antisolvent coating methods. Triflusal release from Eudragit-coated aerogel particles was compared with the dissolution profiles recorded for pristine triflusal and for triflusal impregnated into polymer or non-coated aerogel particles. The release profiles were determined by high-performance liquid chromatography. Eudragit-coated materials presented an intermediate drug-release rate between this obtained for the infused polymer and that of the impregnated aerogel particles. Diffusion-governed mechanisms were found for the studied aerogel-like systems after fitting the release data to both Korsmeyer-Peppas and Baker-Lonsdale equations. The major advantage of the compressed CO_2 antisolvent approach was the ability to physically coat very fine particles (<100 nm). Moreover, the stability of the studied drug in water increased after coating.

Keywords Supercritical processing · Nanoparticles · Polymers · Controlled release

N. Murillo-Cremaes · A. Roig (✉) · C. Domingo (✉)
Institut de Ciència de Materials de Barcelona (CSIC),
Campus de la UAB, 08193 Bellaterra, Spain
e-mail: roig@icmab.es
e-mail: conchi@icmab.es

N. Murillo-Cremaes
e-mail: nmurillo@icmab.es

P. Subra-Paternault (✉)
Université Bordeaux, CBMN UMR 5248, Bat B14 bis,
Allée Geoffroy St Hilaire, 33600 Pessac, France
e-mail: subra@enscbp.fr

J. Saurina
Department of Analytical Chemistry, University of Barcelona,
Martí i Franquès 1-11, 08028 Barcelona, Spain

Introduction

Polymer coating of micro- and nanoparticles is presently a widely used technique for powder processing in various important industries, including pharmaceuticals, food, fertilizers, cosmetics, electronics, etc. [1–3]. Most of the coating materials are natural or synthetic polymers [4–6], but fats, lipids, and waxes can also be used for encapsulation [7–9]. Polymer coating usually modify several physical characteristics of the original material, such as hydrophility, appearance, or mechanical strength. Encapsulation can also result in more uniform particle size distribution, smoother surfaces, and enhanced flowability. Regarding the chemical characteristics, coating aids to protect unstable ingredients from external degradation factors, such as moisture, air, or light, and can enhance compatibility and wettability. In the particular case of controlled drug delivery, encapsulation is used to modulate the release rate of an active pharmaceutical ingredient to the organism. Other advantages attained by coating are better dispersion and deagglomeration, as well as enhanced functionality when coated with specific polymers such as polyethylene glycol that gives amphiphilic character and prevent recognition by the immune system [10, 11]. Many of the marketed polymeric drug delivery carriers are adequate for the sustained release of water-soluble drugs. For low water-solubility drugs, polymeric systems could also exhibit a good response but often release the drug very slowly due to its high hydrophobicity. As an alternative, the relevance in controlled drug delivery of inorganic materials such as silica, titania, or magnetic iron oxide

particles, either alone or combined with polymers in hybrid matrices, is increasing [12–14]. Inorganic porous particles are mostly applied to obtain an immediate drug dosage of poorly water-soluble compounds at the desired target site.

The technologies currently used in the industry for coating solid particles, based on either mechanical movement (agitation) or solid fluidization (Wurster process), mainly involve organic solution chemistry and the use of high temperatures to evaporate the solvent [15–17]. In these processes, the replacement of organic solvents with supercritical and compressed carbon dioxide (CO_2) results in an environmentally friendly option with a near-zero waste production. CO_2 is an ideal processing medium at high pressure, because of its relatively mild critical conditions (31.1 °C and 73.8 bar) and generally recognized as safe (GRAS) status. The applicability of the already known supercritical micronization techniques to coating depends primarily on the solubility of the coating material in compressed CO_2 [18, 19]. In general, compressed CO_2 has a limited solvent strength for many polymers of interest. Hence, most of the work performed in coating using compressed CO_2 has been carried out by antisolvent methods [20, 21] and only a few by polymer precipitation from the solvent, as in the rapid expansion of supercritical solutions (RESS) process [22–25]. In a further evolution, the RESS and the fluidized bed technologies have been combined, using supercritical CO_2 as the fluidizing gas and as a solvent [26–31]. The precipitation from gas saturated solutions (PGSS) process and the co-injection route, in which the supercritical CO_2 is dissolved in a polymer to reduce its melting temperature, are used to coat thermally sensitive compounds [32, 33]. However, individual coating is difficult to achieve using these processes, especially for small-sized particles. In a different approach, particles have been coated by in situ dispersion polymerization in supercritical CO_2 [34, 35]. This coating method has shown excellent results for the encapsulation of fine particles; however, it would be severely limited for drug-coating applications due to residual monomers. Spouted bed technology has recently been applied to coat large micrometric silica aerogel particles [36] and surface-initiated polymerization for the coating of aerogel disks with a hydrogel [37].

In previous works, we reported on the supercritical preparation of impregnated drug delivery systems involving triflusal (Trf) drug, based in either homopolymers [38] or aerogel-like silica matrices [39]. Trf is a drug practically insoluble in water and highly unstable at a neutral and alkaline pH. The in vitro release study demonstrated a sustained release prolonged for several days in the polymeric system [38], while more than 80 % of triflusal was dissolved in the media within the first minutes for the aerogel matrices [39]. In this study, we have extended our background in supercritical and compressed CO_2 impregnation and antisolvent precipitation to the deposition of polymeric thin films of Eudragit® RL 100 on the surface of silica aerogel-like fine particles, either as synthetized or previously impregnated with Trf. Two different types of particulate silica were studied: sub-micron size silica particles (SiO_2 300 nm) [40] and magnetite-silica (Fe_3O_4@SiO_2 65 nm) nanospheres [41].

CO_2 antisolvent approaches have often been successfully applied to the coating of micrometric organic and inorganic particles [10, 42–44], although only in some particular cases they are used for the coating of nanometric particles. For example, the compressed antisolvent coating technique was used for the surface modification of superparamagnetic iron oxide nanoparticles of 10–15 nm diameter [45, 46]. The magnetic particles have been long commercialized as contrast agents for magnetic resonance imaging and are coated to reduce magnetic agglomeration [47]. In our study, the used superparamagnetic Fe_3O_4 nanoparticles embedded as a core into a SiO_2 matrix (Fe_3O_4@SiO_2) present low magnetic agglomeration [41]. In this work, both the batch gas antisolvent (GAS) and the semicontinuous precipitation compressed antisolvent (PCA) techniques were used for particle encapsulation. Results showed that particle encapsulation was achieved in both cases. In vitro characterization by high-performance liquid chromatography (HPLC) proved that the deposited coating acted as a drug-release barrier, thus obtaining delivery rates that are in between those attained with polymeric systems and uncoated aerogel particles. Moreover, drug stability in water increased in the hybrid matrix constituted by aerogel particles and polymer with respect to the rest of studied encapsulation systems.

Experimental

Materials

2-Acetyloxy-4-(trifluoromethyl) benzoic acid or triflusal (Trf) was kindly donated by Uriach S.A., Spain. Eudragit® RL 100 amorphous polymer (Evonik Rohm Pharma Polymer, Degussa) was selected as the coating element and was kindly supplied by IMCD, France. It is a copolymer of acrylate and methyl methacrylate with a low content of methacrylic acid ester and quaternary ammonium groups. This polymer is water insoluble, but sweallable, with a relatively high permeability that comes from the presence of the ammonium salt. Sub-micron silica aerogel-like particles (AP) and magnetite-silica composite nanoparticles (AP_{Fe}), with diameters of 300 and 65 nm, respectively, were synthesized in our laboratory by hydrolysis and polycondensation of tetramethylorthosilicate (TMOS, 98 %, Sigma-Aldrich) and high temperature supercritical drying, according to the procedures described elsewhere [40, 41]. These particles had a surface area of near 200 $m^2\ g^{-1}$ and a pore volume of ca. 0.07 $cm^3\ g^{-1}$. Some AP_{Fe} nanoparticles were impregnated with Trf by a supercritical method, as previously reported [39], thus obtaining Trf@AP_{Fe} nanoparticles. The Trf loading was in the order of ca. 4 wt% of

Trf. Acetone (99.8 wt% purity, VWR) was used to suspend the inorganic nanoparticles and CO_2 (industrial grade, Air Liquid) as the antisolvent.

CO_2 antisolvent processes

First experiments were performed in a GAS home-made batch apparatus, consisting of a 0.5-L autoclave that at the bottom has a membrane filter of 0.22 μm placed on the top of a stainless steel frit (5 μm mesh). The setup is described elsewhere in detail [48, 49]. In the batch approach, compressed CO_2 was introduced into the vessel that contained the acetone suspension of sub-micron silica particles and the dissolved polymer. The vessel was equipped with a stirrer plunged in the solution, thus maintaining the particles in suspension. In a typical GAS experiment, AP and drug were weighed in a mass ratio of 1.1:1.7 (ca. 0.25 g of Trf) and mixed with 40 mL of acetone. The obtained mixture was soaked overnight under mild conditions of stirring, previous to Eudragit addition in a polymer:silica mass ratio of 1:1.1. The temperature of the vessel was controlled by heating jackets and maintained at 26 °C during the polymer precipitation step. Compressed CO_2 was added resulting in a gradual increase of the pressure in the chamber up to 100 bar. After 1 h, the exit valve was opened, and the product was washed at 30 °C with a fresh flow of CO_2.

A second set of experiments, aiming at coating the smallest silica particles (65 nm), was performed using the PCA semicontinuous approach. The equipment is fully described elsewhere [48]. In the PCA technique, the liquid phase involving dispersed silica nanoparticles and a dissolved polymer was sprayed into a continuous feed of CO_2. In the PCA1 experiment, the acetone suspension had concentrations of pre-impregnated Trf@AP_{Fe} and polymer of 4 and 8 mg mL^{-1}, respectively. The mixture was sonicated during 15 min before pumping. In the PCA2 experiment, a weighted amount of Trf calculated to reach a concentration of 6.5 mg mL^{-1} was added to acetone containing dispersed AP_{Fe} particles (5 mg mL^{-1}) and dissolved polymer (20 mg mL^{-1}). The high pressure autoclave was first heated at 30 °C and filled with CO_2 at a pressure of 90 bar, and then, the acetone suspension was sprayed into the vessel at a flow rate of 1.5–2.0 mL min^{-1}. A capillary nozzle (180 μm diameter) was used to deliver the suspension. Liquid CO_2 was continuously pumped to the vessel at a rate of 15–25 g min^{-1} during acetone injection and, afterwards, for 1 h to wash the obtained product. The coated material was recovered on a 5-μm filter overtopped by two membranes of 0.22 μm placed at the bottom of the autoclave.

Characterization

Fourier transform infrared spectroscopy (FTIR, Perkin Elmer Spectrum One instrument) was used to monitor the success of the processing technique by signaling the presence of the different components (Trf, SiO_2, and the polymer). Thermogravimetric analysis (TGA, system NETZSCH-STA 449F1) was used to estimate the percentage of organic components in the recovered products. Morphological characterization was based on scanning (SEM, Hitachi S570) and transmission (TEM, JEOL JEM-1210) electron microscopies. Mean particle size and polydispersity of each system were obtained by using the ImageJ software package, adjusting the particle size histogram obtained from 200 counts in the TEM images to a Gaussian distribution. Drug-release kinetic profiles were monitored using a Trf-established HPLC method described elsewhere [50]. The delivery of the active component was studied at pH 2 in a 0.01 M HCl medium, fixing the stirring rate and temperature at 60 rpm and 37 °C, respectively. Acid pH was chosen to simulate physiological conditions at the stomach. The metabolite of Trf (4-(trifluoromethyl) salicylic acid, HTB) was also quantified. To calculate the amount of impregnated drug, both the Trf and the HTB contributions were considered. The kinetic curves were monitored chromatographically, measuring the UV absorption at 280 nm, to obtain the corresponding delivery profiles. Total loading was obtained from HPLC data at 100 % release.

Results and discussion

The antisolvent process is based on solute precipitation occurring when compressed CO_2 and an organic liquid phase that contains the solute come into contact [51, 52]. The interdiffusion of the organic solvent and CO_2 creates conditions of solute supersaturation in the organic phase, since the newly formed CO_2 solvent mixture exhibits lower solubilization ability than that of the pure solvent. Besides the precipitation of a single specie, the formation of complex mixtures can be also carried out through the CO_2 antisolvent coprecipitation of two or more solutes dissolved in the liquid phase [44, 53]. In the process used in this work, fine aerogel-like particles were suspended in a liquid solution containing the dissolved polymer. The CO_2 addition provoked the precipitation of the polymer embedding the inorganic particles and giving place to hybrid products. The used experimental conditions are shown in Table 1 together with some end-product characteristics. Under working conditions, the process yield was typically below 50 wt%, likely due to the high solubility of Trf and Eudragit in acetone. The yield was also reduced due to the nanometric character of the inorganic nanoparticles that could easily bypass the used filter at the bottom of the reactor. Moreover, Trf has a relatively high solubility in compressed and supercritical CO_2. For instance, a mole fraction of 3×10^{-2} was measured at 200 bar and 35 °C [38]. Experiments were performed at temperature lower than the critical temperature

Table 1 Composition of the processed slurry and recovered powder, in regard to polymer, silica matrix, and triflusal drug, for the performed antisolvent experiments

Sample	Matrix composition before coating		Slurry composition	Composition of as-recovered samples		
	Silica aerogel	Trf (wt%)	Eudragit:silica:Trf ratio [mg mL^{-1}]	Silica (wt%)	Trf (wt%)	Eudragit (wt%)
GAS1	AP	0	1:1.1:1.7	60	1	39
PCA1	Trf@AP_{Fe}	4.1	1:0.5:0.05	43	1	56
PCA2	AP_{Fe}	0	1:0.25:0.3	47	2	51

of CO_2 to reduce drug solubility in the solvent mixture and to prevent polymer swelling in the liquid phase. Organic compounds solubility in CO_2+solvent mixtures increase generally with temperature [51, 54], thus processing at low temperature reduced the risk of losing the Trf drug by dissolution. Regarding the mixing behavior of the solvent and CO_2, 3D simulation showed that the mixing plume did not differ notably in the interval from 25 to 45 °C, since convection and not diffusion is the mechanism that dominates mass transfer [51].

When performing the PCA experiments, a part of the coated material was found stacked to the filter as a cake due to the continuous flow. The rest of the product was recovered from the body of the reactor as a free-flowing powder. In Fig. 1a, a SEM picture of the filter cake product is shown, in which aggregates of nanoparticles entrapped in a polymeric mass can be observed. SEM (Fig. 1b) and TEM (Fig. 1c) characterization of the as-recovered flowing powder for the PCA1 experiment showed that it consisted of small-agglomerated entities immersed in a continuous polymer film. The flowing powder can be further dispersed by rinsing it with a minimum amount of a proper solvent (acetone, ethanol, or methanol) to eliminate the excess of polymer (Fig. 1d). A liquid solvent washing of the excess polymer was not strictly necessary for controlled drug delivery applications; however, it was considered desirable to reduce particle aggregation while still having a polymer coating, as was later confirmed by FTIR and TGA measurements.

Batch GAS approach was applied to modify the surface of the 300-nm AP particles. The feasibility of this precipitation-

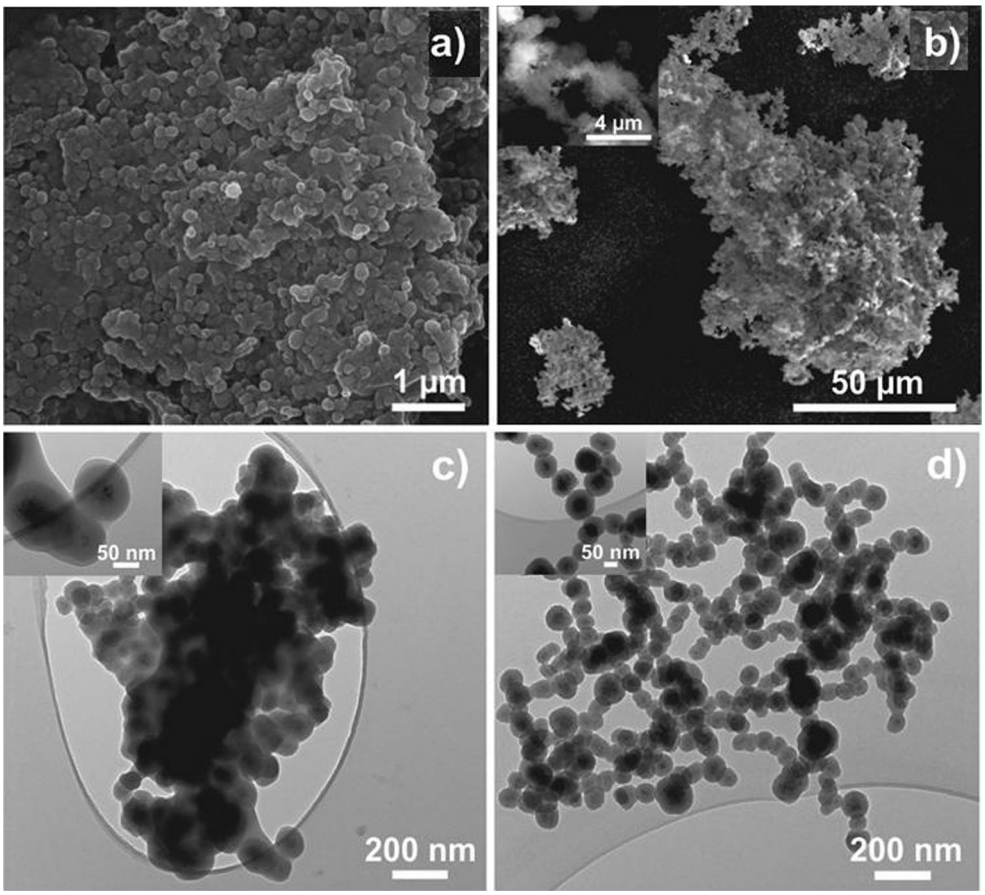

Fig. 1 Images of the collected product from experiment PCA1: SEM pictures of **a** the cake and **b** the as-recovered powder, and TEM images of the flowing powder **c** as-recovered and **d** after rinsing it with methanol

on-slurry technique has been demonstrated previously for micrometric particles [49]. This approach was selected preferably to the semicontinuous PCA mode to coat the largest silica particles that are difficult to pump avoiding sedimentation. The PCA approach could be applied only for the coating of the nanometric 65-nm AP_{Fe} particles, avoiding flow instabilities and nozzle plugging occurring when pumping large particles. For Trf pre-impregnated samples, it was observed that the drug loading was reduced after antisolvent processing, likely due to partial dissolution of the drug in both the compressed CO_2 and in the liquid phase. To avoid this problem, GAS experiments were performed starting from a non-impregnated AP sample that was soaked overnight with a solution of Trf in acetone (GAS1 experiment). The performed soaking step was envisioned as a way to infiltrate the drug into the silica pores [55]. Using the PCA approach, samples were prepared either directly from a triflusal pre-impregnated material, Trf@AP_{Fe}, (PCA1 experiment) or by first soaking pristine AP_{Fe} nanoparticles in acetone with Trf overnight (PCA2 experiment).

Sample composition

FTIR spectroscopy was used to monitor the presence of the different components in the precipitated products involving Trf drug, silica matrix, and Eudragit polymer as a coating agent. The spectra of the different products obtained following the different antisolvent routes are shown in Fig. 2. The as-recovered samples were rinsed with methanol before analysis. The most distinctive band in the spectrum of Eudragit was the C=O vibration appearing at ca. 1,725 cm^{-1}. Moreover, the spectra of the polymer exhibited the characteristic bands of the asymmetric and symmetric alkyl stretching modes at 2,990 and 2,950 cm^{-1}, respectively. The corresponding absorbance of bending vibrations was shown as a shoulder at ca. 1,480 cm^{-1} and as two peaks at ca. 1,445 and 1,385 cm^{-1}. For all the studied silica matrices, intense absorption bands

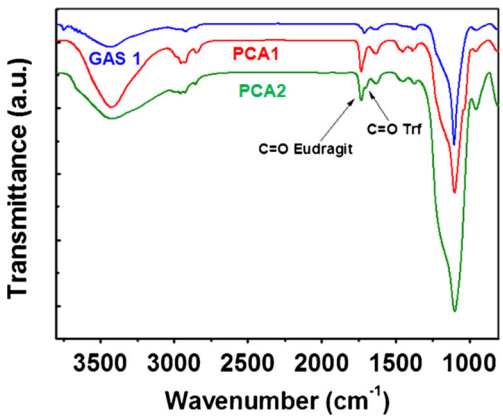

Fig. 2 FTIR spectroscopic analysis of the Eudragit-coated products, indicating the C=O carbonyl functionality for the polymer and, tentatively, also for the drug

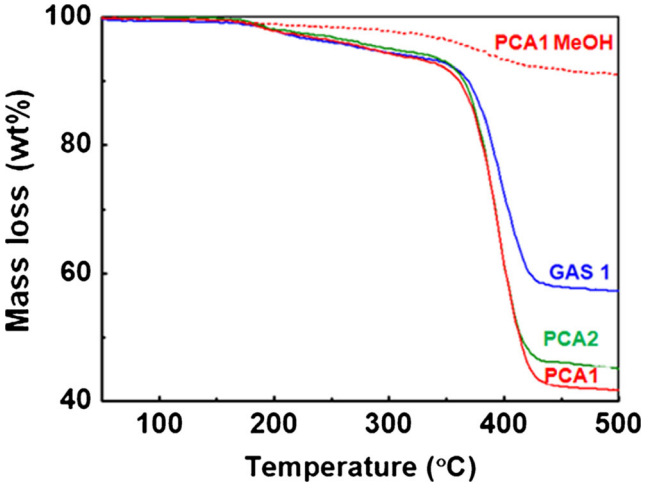

Fig. 3 Thermal analysis of the as-recovered-coated powder in the GAS1, PCA1, and PCA2 experiments, and sample PCA1 also after rinsing it with methanol (PCA1 MeOH)

appeared in the 900–1,200 cm^{-1} region, which corresponded to the stretching vibrations of the O–Si–O bond in the SiO_4 tetrahedrons of the aerogel skeleton. The band at 1,620–1,630 cm^{-1} was due to the bending frequency of molecular water adsorbed in the silica. The broad band from the free O–H stretching vibration was observed in the range of 3,600–3,100 cm^{-1}. The useful FTIR region of solid Trf/HTB contained bands at 1,770 and 1,685 cm^{-1} corresponding to the carbonyls (C=O). The presence of Trf in the coated matrices was difficult to assess, due to the low percentage of drug in the samples. However, for some samples, the Trf could be tentatively monitored by the C=O band of the ester appearing at a frequency near 1,770 cm^{-1}, as a shoulder of the more intense carbonyl band associated to the polymer occurring at a slightly higher frequency (1,725 cm^{-1}).

The quantification of the organic and inorganic phases was performed by sample pyrolysis using TGA analysis (Fig. 3). The thermogravimetric curves obtained indicated that Eudragit polymer decomposed in the temperature interval 350–430 °C. The lost of Trf occurred in the range 150–350 °C. However, the amount of Trf in the samples was too small to be quantified following this procedure. The residue lasting after heating up to 450 °C was assigned to the

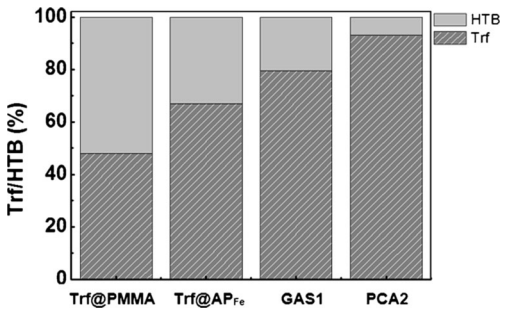

Fig. 4 Percentage of Trf and HTB in the studied matrices after 6 months of storage

inorganic phase. In the GAS1 sample, the percentage value of the residue at 450 °C corresponded to ca. 60 wt% of the total composite mass, while in the PCA precipitated products, this percentage was reduced to values of less than 50 wt%. After rinsing PCA1 sample with methanol, the percentage of polymer was reduced to values of 10–20 wt%.

The preservation of the Trf form, in terms of hydrolysis to HTB, inside the silica matrices during preparation and storage was studied and compared with the behavior observed for the pure drug, the Trf@AP_{Fe} sample before coating and with a polymeric system involving Trf impregnated in polymethylmethacrylate particles (sample Trf@PMMA). The transformation was evaluated after 6 months of storing the samples under ambient conditions, i.e., 21 °C and 60–65 % relative humidity [39]. The amount of either Trf or HTB was determined from the corresponding chromatographic peaks at the initial stages of the release. Figure 4 shows that the Trf transformation for the different samples was of more

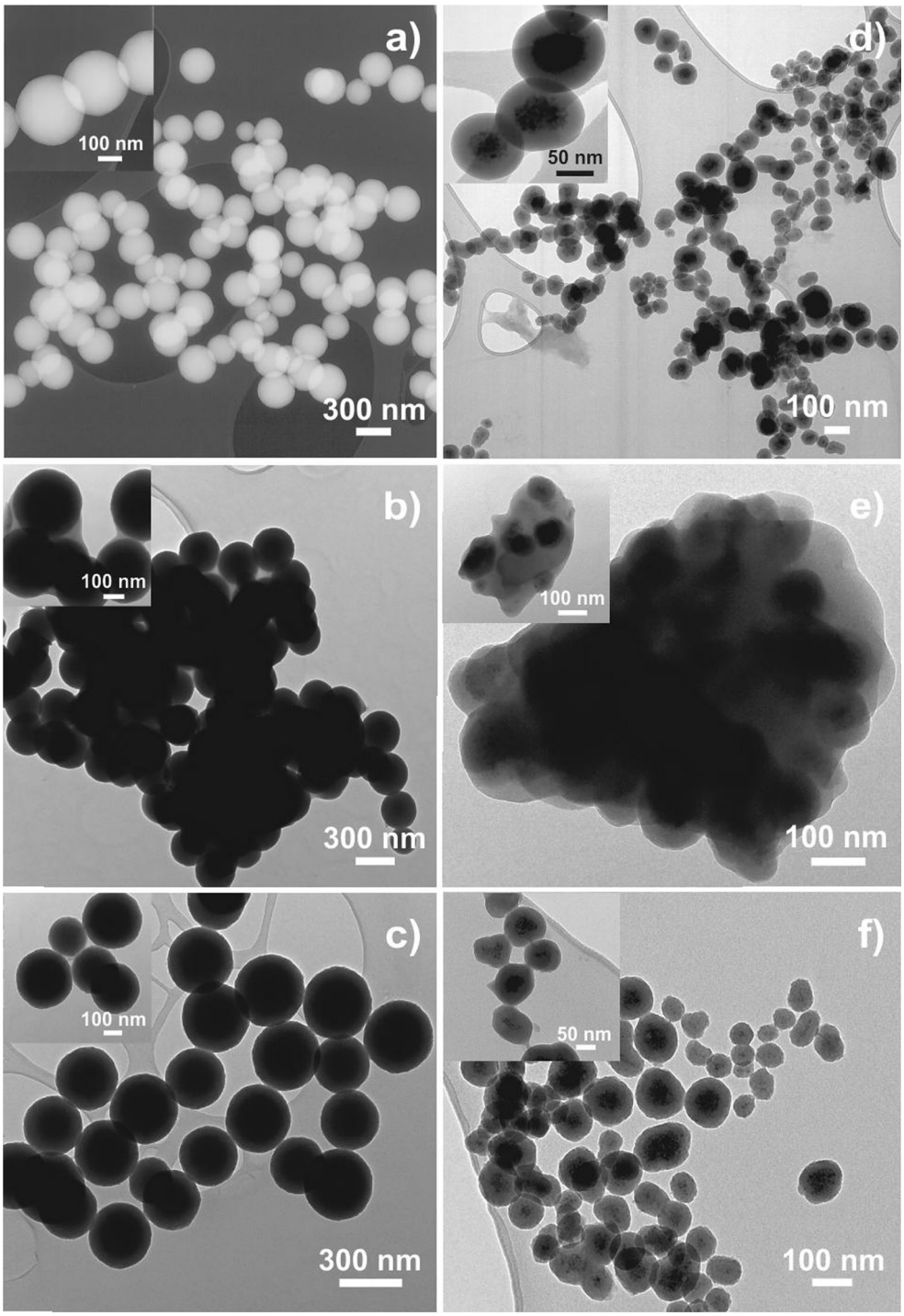

Fig. 5 TEM images of the following: **a** pristine AP particles, **b** as-recovered GAS1 sample, **c** GAS1 sample rinsed with methanol, **d** pristine AP_{Fe} nanoparticles, **e** as-recovered PCA2 sample, and **f** PCA2 sample rinsed with methanol

than 50 % for the PMMA-based matrix to less than 5 % for the Eudragit-coated AP_{Fe} particles. An intermediate situation was observed for the uncoated Trf@AP_{Fe} and Eudragit-coated AP samples, which had hydrolysis degrees of 20–30 %. In principle, the preservation of the ester form present in non-hydrolyzed Trf could be presumed for hydrophobic polymeric matrices. However, hydrophilic environments, such as the one existent inside of the pores of the silica aerogel-like particles, preserved the water-sensitive drug more efficiently than the PMMA beads. This finding was attributed to the acidity that silica materials provided to the adsorbed water. Trf is a drug with a relatively high stability in acid media [50]. After impregnation, the PMMA matrix would have an internal porosity induced by CO_2 swelling [38]. This feature allowed the incorporation of neutral water to the matrix, which led to a high hydrolysis degree of the Trf drug. For the inorganic particles, the coating with Eudragit likely avoided the diffusion of water into the material, minimizing the subsequent drug hydrolysis.

Sample morphology

The bare AP matrix consisted of spherical fine particles of 300-nm mean diameter with a 9 % polydispersity (Fig. 5a). The inset in Fig. 5a evidences that the spheres were not aggregated, and necking between them were not observed. After GAS precipitation, the as-recovered particles were clearly embedded in a continuous mass of polymer (Fig. 5b). The thickness of the polymer film could be reduced by rinsing the sample with methanol (Fig. 5c), thus producing an easily flowable-coated powder. The presence of the polymer after rinsing was not easily seen in the images, and only a thin layer of the organic material connecting the particles was visible (see the inset in Fig. 5c).

The AP_{Fe} particulate matrix was characterized by a mean diameter of 65 nm and 20 % size dispersion (Fig. 5d). The nanocomposite was constituted by a core of magnetite nanoparticles (ca. 6 nm diameter) surrounded by a shell of porous silica. This core/shell structure is easily distinguishable in the image inset of Fig. 5d. After loading with Trf, the particles did not show morphological differences (image not shown). Similar behavior to that explained for GAS1 sample was observed for PCA1 and 2 samples. The PCA coating process produced particles embedded in a polymer mass (Fig. 5e), which was partially eliminated with methanol giving place to almost individually coated particles (Fig. 5f). The polymer can be still observed as a thin layer that covers and attaches the nanoparticles together (inset of Fig. 5f).

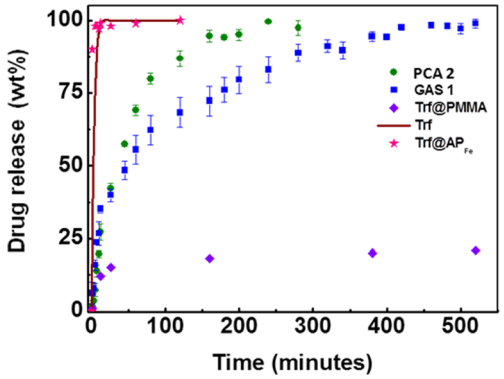

Fig. 6 Drug delivery profiles for pure Trf (*solid line*), Trf pre-impregnated PMMA (Trf@PMMA), and AP_{Fe} (Trf@AP_{Fe}) samples, and powder recovered from GAS1 and PCA2 experiments

Drug-release profiles

The percentage of drug loaded in each as-recovered powder was determined by HPLC (Table 1). Obtained values were in the order of 1 wt% for GAS1 and PCA1 samples and of 2 wt% for PCA2 sample. For samples GAS1 and PCA2, release kinetics were followed under gastric pH conditions (Fig. 6). The carboxylic acid of the Trf molecule is protonated at the acid stomach pH, and the drug is completely absorbed before reaching the intestine. Drug dissolution profile of pure Trf is also shown in the figure for comparison, together with the Trf release curves of samples Trf@AP_{Fe} and Trf@PMMA. For uncoated silica aerogel nanospheres (Trf@AP_{Fe}), the drug release in acidic pH occurred almost instantaneously, and 95 % of the drug was dissolved within the first minute. At pH=2, pure triflusal was fully dissolved in a period of 15 min. In contrast, the slowest release kinetics was obtained for the sample Trf@PMMA. In this case, the delivery of Trf from the sample to gastric medium lasted several days, having only the 18 % released in the first 60 min. The measured drug delivery profiles of the coated samples GAS1 and PCA2 were intermediate between those of Trf@AP_{Fe} (fastest kinetics) and Trf@PMMA (slowest kinetics). For coated samples, ca. 25 % of the drug was dissolved during the first 10 min, and a progressive release of the remaining 75 % occurred during the next 5–8 h. For instance, at 60 min, the released percentages were of 55 and 70 % for GAS1 and PCA2 samples, respectively. Reasons of prolonged released in the coated systems were related to the necessity of swelling the polymer before diffusion

Table 2 Release parameters estimated from the fits of the experimental data to the Korsmeyer-Peppas model for samples GAS1 and PCA2

Sample	R^2	n	a (h^{-n})
GAS1	0.9838	0.49	0.55
PCA2	0.9965	0.42	0.92

and the long diffusion channels that the drug molecules have to follow to reach the bulk solution.

To better understand the mechanism of the drug delivery from the Eudragit-coated aerogel-like silica nanoparticles, the release data was fitted in the light of two different mathematical models. The first one, the Korsmeyer-Peppas model [56, 57], is a simple semi-empirical model which follows Eq. (1) and includes the possibility of a burst effect:

$$\frac{M_t}{M_\infty} = at^n + b \tag{1}$$

where M_t represents the amount of the drug released at time t; M_∞, the total amount of drug released over a long period of time (it is considered equivalent to the drug loading); a, the kinetics constant that is related to structural and geometrical characteristics of the carrier; t, the elapsed time; n, the release exponent, indicative of the drug-release mechanism; and b, the parameter that introduces the burst effect. This model is commonly used to describe the drug release from polymeric systems and when the kinetics of the process is unknown. The second model is the Baker-Lonsdale [57] that interprets the diffusion of the drug from a spherical matrix, being adjusted to the expression shown in Eq. (2):

$$f_{i=\frac{3}{2}\left[1-\left(1-\frac{M_t}{M_\infty}\right)^{2/3}\right]-\frac{M_t}{M_\infty}=kt} \tag{2}$$

where M_t is the drug-released amount at time t and M_∞ is the amount of drug released at an infinite time. For a heterogeneous system with structural features that influence the drug discharge mechanism, k can be written as depicted in Eq. (3):

$$k = \frac{3D_f K C_{fs}}{r_0^2 \tau} \tag{3}$$

being D_f the diffusion coefficient, K the drug specific volume, C_{fs} the drug solubility in the liquid surrounding the matrix, r_0 the radius of the spherical matrix, and τ the tortuosity factor of the system. The use of this approach requires the total drug loading to be greater than its solubility in the matrix.

The dissolution data of drug for samples GAS1 and PCA2 were both fitted to Eq. (1) and for sample GAS1 also to Eq. (2). For Eq. (1), only the first 60 % of the cumulative release points was considered, as the Korsmeyer-Peppas model demands. Correlation coefficients (R^2) were employed to evaluate the quality of the fit. In Table 2, the "n" values, the kinetic constants and the correlation coefficients resulting from fitting the curves with the Korsmeyer-Peppas equation are presented" for clarity sake of the text. On the basis of this model, reasonable values of R^2 were obtained, especially for the case of PCA2 sample (0.9965). In addition, the n exponents were determined to be equal to 0.42 and 0.49 and the kinetic constants to 0.92 and 0.55 for PCA2 and GAS1 samples, respectively (see Fig. 7a, b). According to these results, the drug was released by a Fickian diffusion mechanism in PCA2 sample. The sample GAS1 did not seem to be governed by a Fick's law [58] but could be described by anomalous transport, as Peppas et al. determined for spherical polymeric matrices [59]. The release data of GAS1 sample was also fitted to the Baker-Lonsdale equation, obtaining a correlation coefficient value of 0.9888 (Fig. 7c).

Conclusions

Compressed CO_2 antisolvent route was here presented as a versatile approach for coating fine particles and preparing hybrid composites made of aerogel-like particles, a polymeric coating, and an active pharmaceutical ingredient. For relatively large particles (300 nm), the coating was based on mixing an acetone slurry of aerogel nanoparticles and dissolved polymer with pressurized CO_2 in a batch antisolvent mode (GAS method). A semicontinuous antisolvent mode (PCA method) could be applied to encapsulate nanometric aerogel particles

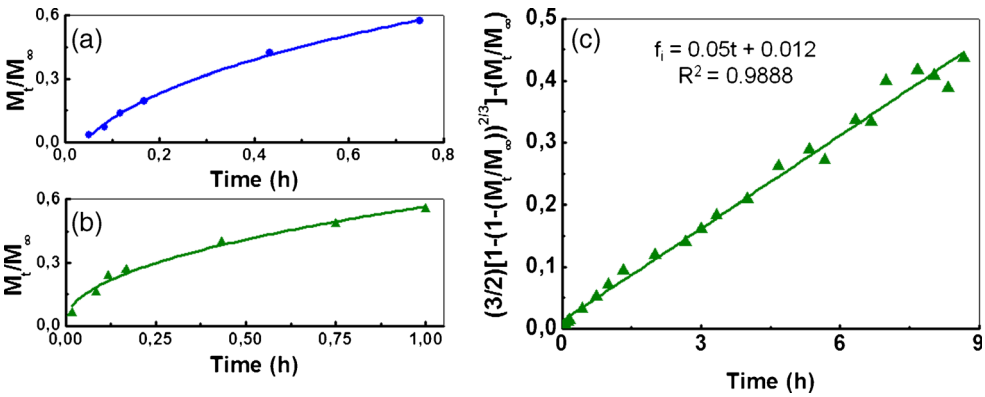

Fig. 7 Drug-release data fitted with the Korsmeyer-Peppas equation for the following: **a** PCA2 and **b** GAS1 samples, and with the Baker-Lonsdale equation for **c** GAS1 formulation. *Symbols* correspond to experimental data and *solid lines* to fitted profiles

(65 nm). The coating was performed without any prefunctionalization of the surface of the silica nanoparticles, although, in some cases, they were supercritically pre-impregnated with the therapeutic agent. Our results showed that sub-micron and nanometric porous silica particles were successfully coated by the polymer Eudragit forming loose agglomerates while simultaneously incorporating the drug. At low pH, triflusal-loaded aerogel nanoparticles released almost 100 % of the drug in the first 5 min, whereas coating with Eudragit enabled a significant reduction to less than 25 % in the first 10 min and prolonging further the release to several hours. In addition, the kinetics of the release was shown to obey the Baker-Lonsdale model indicating a diffusion-controlled delivery of the drug for the sample obtained using the GAS method and the Korsmeyer-Peppas model for the sample prepared by PCA, exhibiting a Fickian diffusional mechanism. Compressed CO_2 antisolvent processes are environmentally friendly techniques for fine particles encapsulation/coating with diverse solutes, which have applications as high-added-value pharmaceutical products in relation with their surface chemistry and delivery characteristics.

Acknowledgments This work was partially funded by the Spanish Government (MAT2010-18155, MAT2012-35324, MAT2012-35161), the Generalitat de Catalunya (2009SGR203 and 2009SGR666), and the COST Action MP1202. N. Murillo-Cremaes acknowledges the FPU grant from the Spanish Education Ministry.

References

1. Feng W, Patel SH, Young M-Y, Zunino JL III, Xanthos M (2007) Smart polymeric coatings-recent advances. Adv Polym Technol 26: 1–13
2. Aguirre M, Paulis M, Leiza JR (2013) UV screening clear coats based on encapsulated CeO_2 hybrid latexes. J Mater Chem A 1: 3155–3162
3. Nam J, Won N, Bang J, Jin H, Park J, Jung S, Jung S, Park Y, Kim S (2013) Surface engineering of inorganic nanoparticles for imaging and therapy. Adv Drug Deliv Rev 65:622–648
4. Yan FY, Gross KA, Simon GP, Berndt CC (2003) Peel-strength behavior of bilayer thermal-sprayed polymer coatings. J Appl Polym Sci 88:214–226
5. Skirtach AG, Volodkin DV, Möhwald H (2010) Bio-interfaces-interaction of PLL/HA thick films with nanoparticles and microcapsules. Chem Phys Chem 11:822–829
6. Leyton P, Domingo C, Sanchez-Cortes S, Campos-Vallette M, Garcia-Ramos JV (2005) Surface enhanced vibrational (IR and Raman) spectroscopy in the design of chemosensors based on ester functionalized p-tert-butylcalix[4]arene hosts. Langmuir 21:11814–11820
7. Gomes JFPS, Rocha S, Do Carmo Pereira M, Peres I, Moreno S, Toca-Herrera J, Coelho MAN (2010) Lipid/particle assemblies based on maltodextrin-gum arabic core as bio-carriers. Colloids Surf B: Biointerfaces 76:449–455
8. SarkarR PP, Mahato M, Kamilya T, Chaudhuri A, Talapatra GB (2010) On the origin of iron-oxide nanoparticle formation using phospholipid membrane template. Colloids Surf B: Biointerfaces 79:384–389
9. Vezzù K, Campolmi C, Bertucco A (2009) Production of lipid microparticles magnetically active by a supercritical fluid-based process. Int J Chem Eng 781247:1–9
10. Marre S, Cansell F, Aymonier C (2008) Tailor-made surface properties of particles with a hydrophilic or hydrophobic polymer shell mediated by supercritical CO_2. Langmuir 24:252–258
11. Orts-Gil G, Natte K, Thiermann R, Girod M, Rades S, Kalbe H, Thünemann AF, Maskos M, Österle W (2013) On the role of surface composition and curvature on biointerface formation and colloidal stability of nanoparticles in a protein-rich model system. Colloids Surf B: Biointerfaces 108:110–119
12. Roca AG, Costo R, Rebolledo AF, Veintemillas-Verdaguer S, Tartaj P, González-Carreño T, Morales MP, Serna CJ (2009) Progress in the preparation of magnetic nanoparticles for applications in biomedicine. J Phys D Appl Phys 42:224002
13. Sanchez C, Belleville P, Popall M, Nicole L (2011) Applications of advanced hybrid organic–inorganic nanomaterials: from laboratory to market. Chem Soc Rev 40:696–753
14. Murakami T, Tsuchida K (2008) Recent advances in inorganic nanoparticle-based drug delivery systems. Mini-Rev Med Chem 8: 175–183
15. Domingo C, Saurina J (2012) An overview of the analytical characterization of nanostructured drug delivery systems: towards green and sustainable pharmaceuticals. Anal Chim Acta 744:8–22
16. Fan J, Chen S, Gao Y (2013) Coating of gold nanoparticles with peptide molecules via a peptide elongation approach. Colloids Surf B: Biointerfaces 28:199–207
17. Ebrahiminezhad A, Ghasemi Y, Rasoul-Amini S, Barar J, Davaran S (2013) Preparation of novel magnetic fluorescent nanoparticles using amino acids. Colloids Surf B: Biointerfaces 102:534–539
18. Domingo C, Vega A, Fanovich MA, Elvira C, Subra P (2003) Behavior of poly(methyl methacrylate)-based systems in supercritical CO_2 and CO_2 plus cosolvent: solubility measurements and process assessment. J Appl Polym Sci 90:3652–3659
19. Roy C, Vega-González A, García-González CA, Tassaing T, Domingo C, Subra-Paternault P (2010) Assessment of $scCO_2$ techniques for surface modification of micro- and nanoparticles: process design methodology based on solubility. J Supercrit Fluids 54:362–368
20. Cansell F, Aymonier C (2009) Design of functional nanostructured materials using supercritical fluids. J Supercrit Fluids 47:508–516
21. Seremeta KP, Chiappetta DA, Sosnik A (2013) Poly(ε-caprolactone). Eudragit® RS 100 and poly(ε-caprolactone)/Eudragit® RS 100 blend submicron particles for the sustained release of the antiretroviral efavirenz. Colloids Surf B: Biointerfaces 102:441–449
22. Kim J-H, Paxton TE, Tomasko DL (1996) Microencapsulation of naproxen using rapid expansion of supercritical solutions. Biotechnol Prog 12:650–661
23. Mishima K, Matsuyama K, Tanabe D, Yamauchi S, Young TJ, Johnston KP (2000) Microencapsulation of proteins by rapid expansion of supercritical solution with a nonsolvent. AIChE J 46:857–865
24. Glebov EM, Yuan L, Krishtopa LG, Usov OM, Krasnoperov LN (2001) Coating of metal powders with polymers in supercritical carbon dioxide. Ind Eng Chem Res 40:4058–4068
25. Ovaskainen L, Rodriguez-Meizoso I, Birkin NA, Howdle SM, Gedde U, Wa gberg L, Turner C (2013) Towards superhydrophobic coatings made by non-fluorinated polymers sprayed from a supercritical solution. J Supercrit Fluids 77:134–141
26. Vogt C, Schreiber R, Werther J, Brunner G (2004) Coating of particles in a fluidized bed operated at supercritical fluid conditions. Chem Eng Technol 27:943–945
27. Tsutsumi A, Nakamoto S, Mineo T, Yoshida K (1995) A novel fluidized-bed coating of fine particles by rapid expansion of supercritical fluid solutions. Powder Technol 85:275–278

28. Wang TJ, Tsutsumi A, Hasegawa H, Mineo T (2001) Mechanism of particle coating granulation with RESS process in a fluidized bed. Powd Technol 118:229–235
29. Kröber H, Teipel U (2005) Microencapsulation of particles using supercritical carbon dioxide. Chem Eng Process 44:215–219
30. Rodríguez-Rojo S, Marienfeld J, Cocero MJ (2008) RESS process in coating applications in a high pressure fluidized bed environment: bottom and top spray experiments. Chem Eng J 144:531–539
31. López-Periago AM, Vega A, Subra P, Arguemí A, Saurina J, García-González CA, Domingo C (2008) Supercritical CO_2 processing of polymers for the production of materials with applications in tissue engineering and drug delivery. J Mater Sci 43:1939–1947
32. Calderone M, Rodier E, Lochard H, Marciacq F, Fages J (2008) A new supercritical co-injection process to coat microparticles. Chem Eng Process 47:2228–2237
33. García-González CA, Sampaio da Sousa AR, Argemí A, López Periago AM, Saurina J, Duarte CMM, Domingo C (2009) Production of hybrid lipid-based particles loaded with inorganic nanoparticles and active compounds for prolonged topical release. Int J Pharm 382:296–304
34. Yue B, Yang J, Wang Y, Huang C-Y, Dave R, Pfeffer R (2004) Particle encapsulation with polymers via in situ polymerization in supercritical CO_2. Powd Technol 146:32–45
35. Lock EH, Merchan-Merchan W, D'Arcy J, Saveliev AV, Kennedy LA (2007) Coating of inner and outer carbon nanotube surfaces with polymers in supercritical CO_2. J Phys Chem C 111:13655–13658
36. Alnaief M, Antonyuk S, Hentzschel CM, Leopold CS, Heinrich S, Smirnova I (2012) A novel process for coating of silica aerogel microspheres for controlled drug release applications. Microporous Mesoporous Mater 160:167–173
37. Giray S, Bal T, Kartal AM, Kizilel S, Erkey C (2012) Controlled drug delivery through a novel PEG hydrogel encapsulated silica aerogel system. J Biomed Mater Res 100A:1307–1315
38. López-Periago AM, Argemí A, Andanson JM, Fernández V, García-González CA, Kazarian SG, Saurina J, Domingo C (2009) Impregnation of a biocompatible polymer aided by supercritical CO_2: evaluation of drug stability and drug-matrix interactions. J Supercrit Fluids 48:56–63
39. Murillo-Cremaes N, López-Periago AM, Saurina J, Roig A, Domingo C (2013) Nanostructured silica-based drug delivery vehicles for hydrophobic and moisture sensitive drugs. J Supercrit Fluids 73:34–42
40. Moner-Girona M, Roig A, Molins E (2003) Sol–gel route to direct formation of silica aerogel microparticles using supercritical solvents. J Sol–gel Sci Technol 26:645–649
41. Taboada E, Solanas R, Rodríguez E, Weissleder R, Roig A (2009) Supercritical-fluid-assisted one-pot synthesis of biocompatible core(γ-Fe_2O_3)/Shell(SiO_2) nanoparticles as high reflexivity T2-constrast agents for magnetic resonance imaging. Adv Funct Mater 19:2319–2324
42. García-González CA, Vega-González A, López-Periago AM, Subra-Paternault P, Domingo C (2009) Composite fibrous biomaterials for tissue engineering obtained using a supercritical CO_2 antisolvent process. Acta Biomater 5:1094–1103
43. Wang Y, Dave RN, Pfeffer R (2004) Polymer coating/encapsulation of nanoparticles using a supercritical anti-solvent process. J Supercrit Fluids 28:85–99
44. Wang Y, Pfeffer R, Dave RN (2005) Polymer encapsulation of fine particles by a supercritical antisolvent process. AIChE J 51:440–455
45. Chen A-Z, Kang Y-Q, Pu X-M, Yin G-F, Li Y, Hu J-Y (2009) Development of Fe_3O_4-poly(L-lactide) magnetic microparticles in supercritical CO_2. J Colloid Interface Sci 330:317–322
46. Adami R, Reverchon E (2012) Composite polymer-Fe_3O_4 microparticles for biomedical applications, produced by supercritical assisted atomization. Powd Technol 218:102–108
47. Barbé C, Bartlett J, Kong L, Finnie K, Lin HQ, Larkin M, Calleja S, Bush A, Calleja G (2004) Silica particles: a novel drug delivery system. Adv Mater 16:1959–1966
48. Duarte ARC, Roy C, Vega-González A, Duarte AMM, Subra-Paternault P (2007) Preparation of acetazolamide composite microparticles by supercritical anti-solvent techniques. Int J Pharm 332: 132–139
49. Subra-Paternault P, Vrel D, Roy C (2012) Coprecipitation on slurry to prepare drug-silica-polymer formulations by compressed antisolvent. J Supercrit Fluids 63:69–80
50. Argemí A, López-Periago AM, Domingo C, Saurina J (2008) Spectroscopic and chromatographic characterization of triflusal delivery systems prepared by using supercritical impregnation technologies. J Pharm Biomed Anal 46:456–462
51. Erriguible A, Laugier S, Laté M, Subra-Paternault P (2013) Effect of pressure and non-isothermal injection on re-crystallization by CO_2 antisolvent: solubility measurements, simulation of mixing and experiments. J Supercrit Fluids 76:115–125
52. Kikic I, De Zordi N, Moneghini M, Solinas D (2010) Solubility estimation of drugs in ternary systems of interest for the antisolvent precipitation processes. J Supercrit Fluids 55:616–622
53. Yeo S-D, Kiran E (2005) Formation of polymer particles with supercritical fluids: a review. J Supercrit Fluids 34:287–308
54. Revelli AL, Laugier S, Erriguible A, Subra-Paternault P (2014) High-pressure solubility of naproxen, nicotinamide and their mixture in acetone with supercritical CO_2 as anti-solvent. Fluid Phase Eq 373: 29–33
55. Xu Y, Qu F, Wang Y, Lin H, Wu X, Jin Y (2011) Construction of a novel pH-sensitive drug release system from mesoporous silica tablets coated with Eudragit. Solid State Sci 13:641–646
56. Kim H, Fassihi R (1997) Application of binary polymer system in drug release rate modulation. 2. Influence of formulation variables and hydrodynamic conditions on release kinetics. J Pharm Sci 86: 323–328
57. Costa P, Sousa Lobo JM (2001) Modeling and comparison of dissolution profiles. Eur J Pharm Sci 13:123–133
58. Guo R, Li L-L, Yang H, Zhang M-J, Fang C-J, Zhang T-L, Zhang Y-B, Cui G-H, Peng S-Q, Feng W, Yan C-H (2012) Tuning kinetics of controlled-release in disulfide-linked MSN-folate conjugates with different fabrications procedures. Mater Lett 66:79–82
59. Siepmann J, Peppas NA (2001) Modelling of drug release from delivery systems based on hydroxypropyl methylcellulose (HPMC). Adv Drug Deliv Rev 48:139–157